Dynamic spreading of droplets containing nanoparticles

O. K. Matar, R. V. Craster, and K. Sefiane
[1]*Department of Chemical Engineering, Imperial College London, South Kensington Campus, London SW7 2AZ, United Kingdom*
[2]*Department of Mathematics, Imperial College London, South Kensington Campus, London SW7 2AZ, United Kingdom*
[3]*School of Engineering & Electronics, University of Edinburgh, Mayfield Road, Edinburgh EH9 3JL, United Kingdom*
(Received 1 August 2007; revised manuscript received 2 October 2007; published 26 November 2007)

Recent experiments and models for the spreading of liquids laden with nanoparticles have demonstrated particle layering at the three-phase contact line; this is associated with the structural component of the disjoining pressure. Effects driven by structural disjoining pressures occur on scales longer than the diameter of a particle, below which other disjoining pressure components such as van der Waals and electrostatic forces are dominant. Motivated by these experimental observations, we investigate the dynamic spreading of a droplet laden with nanoparticles in the presence of structural disjoining pressure effects. We use lubrication theory to derive evolution equations for the interfacial location and the concentration of particles. These equations account for the presence of the structural component of the disjoining pressure for film thicknesses exceeding the diameter of a nanoparticle; below such thicknesses, van der Waals forces are assumed to be operative. The resulting evolution equations, for the particle motion and free surface position, are solved allowing for the viscosity to vary as a function of nanoparticle concentration. The results of our numerical simulations demonstrate qualitative agreement with experimental observations of a "step" emerging from the contact line. The results are also relevant to a wide range of other phenomena involving layering, or terraced spreading of nanodroplets, or stepwise thinning of micellar thin films.

DOI: 10.1103/PhysRevE.76.056315 PACS number(s): 47.55.nd

I. INTRODUCTION

The spreading, or thinning, of simple fluids, micellar-, or particle-laden solutions is often accompanied by complex behavior, which manifests itself through "terracing" of the free surface or stepwise thinning. Several notable examples appear in the literature: the terraced spreading of nanodroplets [1,2] showing the advance of the droplet edge as molecular layers, the stepwise thinning of liquid films of micellar solutions [3–12], and, more recently, the formation of "steps" in the detachment of oil droplets by nanoparticle-laden solutions [5,13–16]. There is considerable interest in achieving fundamental, multiscale understanding of spreading and of the interaction between the relevant physics at the microscale, which gives rise to the above-mentioned complex, macroscale phenomena.

The spreading of fluids and, in general, their relationship to any substrate in which they are in contact, is characterized by the interfacial tensions and the film energy; this, in turn, is expressed by the integral over the film thickness of the disjoining pressure. The latter is expressed as a combination of van der Waals, electrostatic, and so-called "structural" forces, as well as steric forces [17,18]. For simple fluids, van der Waals forces and electrostatic effects dominate over very small scales. Stepwise thinning, however, occurs over longer scales and particle layering is observed even at micron scales. Using statistical mechanics, models for the structural component have been developed [14], and applied to equilibrium situations [16]. Complementary to this literature on disjoining pressure are many hydrodynamical studies, based on thin film theory [19,20], such as studies of dewetting phenomena [21,22], rupture [23–25], droplet motion on substrates with wettability gradients [26], and pattern formation [27,28]. The disjoining pressure embodies the interactions between the substrate and fluid and enters the dynamical evolution equations as an energy per unit volume term. However, to the best of our knowledge, in none of these studies have structural disjoining pressures been included in the modeling of thin film dynamics.

The presence of surfactant micellar aggregates or macromolecules in thin liquid films or "nanofluids" can have a drastic effect on the disjoining pressure. In general, the ordering of the nanoparticles between two solid surfaces, when the local film thickness is sufficiently thin to accommodate a few layers of particles, gives rise to particle layering and oscillatory, structural disjoining pressures; these dominate over the shorter range van der Waals and electrostatic forces. Decreasing the magnitude of the separation between the surfaces to less than a particle diameter leads to the expulsion of the nanoparticles from the gap. This particle depletion "force," is entropic in nature, can lead to attraction of the separated surfaces, and is responsible for phase separation in colloidal dispersions [14,17,29–33]. Oscillatory structural forces arise in thin liquid films confined between two smooth solid surfaces in the absence of nanoparticles; in this case, these are termed "solvation" forces since the period of oscillations is similar in magnitude to the diameter of a solvent molecule [32]. These Derjaguin-Landau-Verwey-Overbeek (DLVO) forces have been shown to play a role in the stepwise thinning of foams and colloidal dispersions [3–12], and particle layering was observed over a range of particle diameters: from 5 nm to 2 μm [6,32].

Structural forces can influence the spreading of nanofluids as a result of particle confinement between the air-liquid and liquid-solid interfaces near the contact line. The effect of nanoparticles on the structural component of the disjoining pressure and the spreading process has been investigated in connection with the detachment of oil drops from solid substrates by surfactant solutions within the context of deter-

gency [5,13–16]. The range of these forces was found to greatly exceed that of the van der Waals and electrostatic components [5,14] and the integrated effect of the structural component was shown to give rise to an increase in the spreading coefficient and an enhancement in the spreading rate of a thin aqueous liquid film that promotes the removal of the oil droplet [15].

The oscillatory nature of the structural disjoining pressure component was also recently taken into account in determining the equilibrium profile of the meniscus near the three-phase contact line between the oil and aqueous phases and the solid substrate [14,16]. Chengara *et al.* [16] used an analytical expression for the disjoining pressure, which was developed by Trokhymchuk *et al.* [14] for the structural disjoining pressure based on the Percus-Yevick theory that treats both the confining surfaces and the nanoparticles as hard spheres. This expression accounts for the oscillatory nature of the disjoining pressure due to particle layering, with exponential decay for relatively large thicknesses and a correction which ensured that the Percus-Yevick predictions are consistent with exact statistical mechanical results [33] when the film thickness equals the particle diameter. Chengara *et al.* showed that an increase in nanoparticle concentration and a decrease in the particle diameter and the degree of polydispersity gave rise to an increase in contact line displacement.

In this paper, we revisit the spreading of nanofluids and examine the effect of structural disjoining pressure forces on the *dynamics*. We use lubrication theory and the rapid vertical diffusion approximation to derive a pair of coupled evolution equations for the thin film thickness and nanoparticle concentration. We account for structural disjoining pressure effects using the same expression as that employed by Trokhymchuk *et al.* and Chengara *et al.* [14,16] for film thicknesses greater than or equal to a particle diameter; for small thicknesses, we include van der Waals forces in our description of the disjoining pressure and neglect depletion forces. We focus on the dynamics of an "inner region" near the contact line and obtain numerical solutions of the evolution equations over a wide range of system parameters. We begin by formulating and generating a model for a nanoparticulate laden droplet in Sec. II, with the results from the modeling discussed in Sec. III. The emergence of a foot from the base of the droplet is reminiscent of the terracing often seen in nanodroplet spreading; we consider this as a further example in Sec. III C showing that the terraced structure emerges naturally during the dynamic evolution. We draw to a close with a summary of the results and a discussion of how they relate to some related topics in Sec. IV.

II. FORMULATION

A. Governing equations

We consider a thin film of characteristic thickness $\mathcal{H}$ and length $\mathcal{L}$ (the initial droplet radius) containing monodisperse nanoparticles of diameter d. The viscosity of the film is dependent on the particles' concentration ϕ, and is expressed by the Krieger-Dougherty relationship, $\mu=\mu_0(1-\phi/\phi_m)^{-2}$, for relatively large concentrations (ϕ_m being the concentration at close packing) and $\mu=\mu_0(1+\phi/2)$ for dilute dispersions where μ_0 is the viscosity of the fluid. Alternatively, for relatively large concentrations, we also use $\mu=\mu_0\bar{\mu}(\phi)$ where $\bar{\mu}$ corresponds to a concentration dependence, which represents the recently observed tendency of nanoparticles to lower the viscosity of some particulate suspensions [34]. We use a rectangular coordinate system to describe the two-dimensional film dynamics, (x,z), where x and z correspond to the horizontal and vertical coordinates, respectively; $\mathbf{u}=(u,w)$ is the velocity field in which u and w correspond to its horizontal and vertical components. The film is bounded from below by a solid, rigid, impermeable, and horizontal support, located at $z=0$, and from above by an essentially inviscid gas; the gas-liquid interface is located at $z=h$ and this is endowed with a tension σ, taken to be constant.

We use lubrication theory to study the film dynamics, which exploits the fact that the film aspect ratio is small, $\epsilon \equiv \mathcal{H}/\mathcal{L} \ll 1$ and that inertia is irrelevant. The mass and momentum conservation equations in this limit are

$$u_x + w_z = 0, \quad (p-\Pi)_x = [\mu(\phi)u_z]_z, \quad p_z = 0, \tag{1}$$

where we have neglected gravitational effects. In Eq. (1), p denotes the film pressure due to capillary forces and Π is the disjoining pressure, which will be taken to be ϕ dependent, that will incorporate the structural component. Note that the osmotic contribution to the film pressure P which arises due to the presence of the particles is kept separate; this can enter the problem through its contribution to Π, as will be shown below. The boundary conditions imposed at the substrate are no-slip and no-penetration at the solid wall: $u=w=0$, at $z=0$; tangential and normal stress conditions at $z=h$, which, in the lubrication approximation, reduce to

$$u_z = 0, \quad p = p_0 - \sigma h_{xx}, \tag{2}$$

where p_0 is the pressure in the overlying gas phase; finally there is the kinematic boundary condition, which is expressed by

$$h_t + \left(\int_0^h u dz \right)_x = 0. \tag{3}$$

In order to model intermolecular interactions, we follow an approach recently employed in [14,16], that accounts for the effect of nanoparticles and their confinement on the disjoining pressure in thin films. If the film is sufficiently thick to accommodate several layers of particles, then the layered configuration adopted by the particles gives rise to a disjoining pressure that is oscillatory, and decays, in the local film thickness. Such oscillatory pressures emerge naturally from statistical mechanics [35] when formally considering the interactions between surfaces separated by model fluids. In the present work, we shall use the following form for the disjoining pressure Π:

$$\Pi(h) = \Pi_0 \cos(\omega h + \varphi_2) e^{-\kappa h} + \Pi_1 e^{-\delta(h-d)}, \quad \text{for } h \geq d,$$

$$= -P + \frac{A}{6\pi h^3} + 64 n_0 k T \gamma^2 e^{-\lambda h}, \quad \text{for } 0 < h < d, \tag{4}$$

where we have included van der Waals and electrostatic con-

tributions to the disjoining pressure in addition to depletion forces for $0<h<d$ since they would be present even in the absence of particles. Equation (4), bar the van der Waals and electrostatic components, is the model of Trokhymchuk *et al.* [14]. The various coefficients in this model are derived in Ref. [14] wherein its connections to earlier statistical mechanics and simulations are described. In Eq. (4), $\omega(\phi)$ is a frequency, and $\Pi_1(\phi)=\rho kTZ-P-\Pi_0 c_2$ in which $\rho=6\phi/\pi d^3$ is the number density of the particles; T is the (constant) system temperature (the film is in thermal equilibrium with its surroundings), $Z=e^{\beta\Delta\mu}$ is the compressibility factor wherein $\beta=1/kT$, $\Delta\mu$ is the excess chemical potential (here μ should not be confused with the viscosity) and k is the Boltzmann constant; $c_2=e^{-\kappa d}\cos(\omega d+\phi_2)$ where $\kappa(\phi)$ is a decay coefficient; $\delta=\Pi_1/W_1$ in which $W_1=-2\sigma_s-W_0c_1$, where $\sigma_s(\phi)$ represents the liquid-solid interfacial tension and $c_1=e^{-\kappa d}\cos(\omega d+\varphi_1)$; $\Pi_0(\phi)$, $W_0(\phi)$, $\varphi_1(\phi)$, and $\varphi_2(\phi)$ are ϕ-dependent coefficients; A is the Hamaker constant, n_0 is the bulk concentration of a 1:1 electrolyte; $\gamma=\tanh(e\Psi/4kT)$ in which e is the electronic charge and Ψ is the surface potential of the air-liquid and liquid-solid interfaces; λ is an inverse Debye length.

The dynamics of the particle concentration ϕ are governed by a convective-diffusion equation, which is expressed by

$$\phi_t+u\phi_x+w\phi_z=\mathcal{D}(\phi_{xx}+\phi_{zz}), \tag{5}$$

in which $\mathcal{D}$ is the diffusion coefficient of the nanoparticles. Next, we exploit the slenderness of the film to derive evolution equations that govern its dynamics.

B. Scaling and cross-sectional averaging

It is advantageous to render the governing equations dimensionless using the following scalings: $x=\mathcal{L}\tilde{x}$, $(z,h)=\mathcal{H}(\tilde{z},\tilde{h})$, $t=(L/\mathcal{U})\tilde{t}$, $(p,P,\Pi)=\epsilon^2(\sigma/\mathcal{H})(\tilde{p},\tilde{P},\tilde{\Pi})$ where the tildes have been used temporarily to designate dimensionless variables and are henceforth suppressed; here, $\mathcal{U}=\epsilon^3\sigma/\mu_0$ represents a characteristic velocity. The dimensionless convective diffusion equation governing the evolution of ϕ is then given by

$$\phi_t+u\phi_x+w\phi_z=\frac{1}{\epsilon^2\,\mathrm{Pe}}(\phi_{zz}+\epsilon^2\phi_{xx}), \tag{6}$$

where $\mathrm{Pe}\equiv\mathcal{U}\mathcal{L}/\mathcal{D}$ is a Peclet number characterizing the importance of convective versus diffusive effects. We shall consider $\epsilon^2\,\mathrm{Pe}\ll 1$, which assumes that the fluid layer is so thin that vertical concentration gradients of particles are, to leading order, not important and substitute $\phi(x,z,t)=\phi_0(x,t)+\epsilon^2\,\mathrm{Pe}\,\phi_1(x,z,t)$ into Eq. (6), cf. [36]:

$$\phi_{0t}+u\phi_{0x}=\frac{1}{\mathrm{Pe}}\phi_{0xx}+\phi_{1zz}+O(\epsilon^2\,\mathrm{Pe}). \tag{7}$$

Here, the cross-sectional average of $\phi_1(x,z,t)$ is taken to be zero: $(1/h)\int_0^h\phi_1 dz=0$. The boundary conditions on ϕ are $\phi_z=0$ at $z=0$ and $\mathbf{n}\cdot\nabla\phi_z=0$ where $\mathbf{n}=(-h_x,1)/(1+h_x^2)^{1/2}$ is the outward pointing unit normal from the gas-liquid interface; the latter condition can be rewritten as

$$\phi_z-\epsilon^2h_x\phi_x=0,$$
$$\mathrm{Pe}\,\phi_{1z}-h_x\phi_{0x}=0,\quad \text{at } z=h; \tag{8}$$

whence $\phi_{1z}|_h=h_x\phi_{0x}/\mathrm{Pe}$. Thus an evolution equation for $\phi_0(x,t)$ can be constructed as

$$\phi_{0t}=-\frac{h^2}{3\bar{\mu}(\phi_0)}\phi_{0x}(h_{xx}+\Pi)_x+\frac{1}{\mathrm{Pe}}\frac{(h\phi_{0x})_x}{h}. \tag{9}$$

The x component of the momentum conservation equation can be readily integrated and the boundary conditions applied to give the following expression for u:

$$u=-\frac{1}{\bar{\mu}(\phi_0)}(h_{xx}+\Pi)_x\left(\frac{z^2}{2}-zh\right), \tag{10}$$

where ϕ is now replaced by ϕ_0 to leading order. Substitution of Eq. (10) into the dimensionless version of Eq. (3) yields an evolution equation for the film thickness:

$$h_t=-\left[\frac{h^3}{3\bar{\mu}(\phi_0)}(h_{xx}+\Pi)_x\right]_x, \tag{11}$$

in which the dimensionless disjoining pressure is given by

$$\Pi=\mathcal{C}\left[\bar{\Pi}_0\cos\left(\frac{\bar{\omega}}{\varepsilon}h+\varphi_2\right)e^{-\bar{\kappa}h/\varepsilon}+\bar{\Pi}_1e^{-\bar{\delta}(h-\varepsilon)/\varepsilon}\right],\quad \text{for } h\geq\varepsilon,$$
$$=-\mathcal{C}\frac{6\phi_0}{\pi}\bar{P}+\frac{\mathcal{A}}{h^3}+\mathcal{B}e^{-\bar{\lambda}h},\quad \text{for } 0<h<\varepsilon, \tag{12}$$

where $\varepsilon\equiv d/\mathcal{H}$ is a dimensionless particle diameter, $\mathcal{A}\equiv A/(6\pi\epsilon^2\sigma\mathcal{H}^2)$, $\mathcal{B}\equiv 64n_0kT\gamma^2\mathcal{H}/\epsilon^2\sigma$, and $\mathcal{C}\equiv kT\mathcal{H}/\epsilon^2\sigma d^3$ represent dimensionless parameters that reflect the relative significance of van der Waals, electrostatic, and structural disjoining pressures forces and $\bar{\lambda}\equiv\lambda\mathcal{H}$ is a dimensionless inverse Debye length. The remaining functions in Eqs. (12), $\bar{\Pi}_0(\phi_0)$, $\bar{\omega}(\phi_0)$, $\varphi_2(\phi_0)$, $\bar{\kappa}(\phi_0)$, $\bar{\Pi}_1(\phi_0)$, $\bar{\delta}(\phi_0)$, and $\bar{P}(\phi_0)$ and their functional dependence on ϕ_0 are given in the Appendix.

Equations (9) and (11) govern the dynamics of the nanoparticulate-laden film; the "0" subscript for the leading order particulate concentration ϕ_0 is suppressed henceforth.

C. "Inner" region

In the absence of the disjoining pressure a droplet at equilibrium, in this dimensionless formulation, has a profile $h=(1-x^2)$. Implicit in this is an assumption of how the length scales $\mathcal{H},\mathcal{L}$ relate to the contact angle, i.e., $\theta\sim 2\epsilon\ll 1$, cf. [37,38]. The contact line is at $x=\pm 1$ and our main focus is on its dynamics if structural disjoining pressures are present. Hence we move to the vicinity of the contact line using the following rescalings:

$$h=\varepsilon\hat{h},\quad x=1+\varepsilon\hat{x},\quad t=\varepsilon\hat{t},\quad \Pi=\frac{\hat{\Pi}}{\varepsilon},\quad \mathcal{A}=\varepsilon^2\hat{\mathcal{A}},$$
$$\mathcal{B}=\frac{\hat{\mathcal{B}}}{\varepsilon},\quad \mathcal{C}=\frac{\hat{\mathcal{C}}}{\varepsilon},\quad \mathrm{Pe}=\frac{\hat{\mathrm{Pe}}}{\varepsilon},\quad \bar{\lambda}=\frac{\hat{\lambda}}{\varepsilon}. \tag{13}$$

TABLE I. Magnitude estimates for the dimensionless groups based on the following values for the various physical parameters: $\sigma=0.04-0.072$ N/m, $\mathcal{H}=0.1-2\times10^{-6}$ m, $d=10-50\times10^{-9}$ m, $A=0.1-5\times10^{-20}$ J, $\mathcal{D}=0.01-1\times10^{-9}$ m^2/s, $n_0=0.01$ M, $\Psi=0.03$ V, $\epsilon=0.01$, $T=293$ K, $e=1.60\times10^{-19}$ C, $k=1.38\times10^{-23}$ J/K.

Description	Definition	Range
Reduced particle diameter	$\varepsilon=\frac{d}{\mathcal{H}}$	0.005–0.5
Structural disjoining pressure parameter	$\hat{\mathcal{C}}\equiv\frac{kT}{\epsilon^2\sigma d^2}$	0.005–20.2
van der Waals parameter	$\hat{A}\equiv\frac{A}{6\pi\epsilon^2\sigma d^2}$	0.02–66.3
Electrostatic parameter	$\hat{B}\equiv\frac{64n_0kT\gamma^2d}{\epsilon^2\sigma}$	10^{-25}–10^{-24}
Peclet number	$\hat{\mathrm{Pe}}\equiv\frac{\epsilon^2\sigma d}{\mu_0\mathcal{D}}$	0.04–35

Thus the droplet becomes locally linear, $\hat{h}\sim-2\hat{x}$ for $\hat{x}<0$, which will essentially provide the initial condition for the numerical work below.

Substitution of these rescalings into Eqs. (11) and (9) yields

$$\hat{h}_{\hat{t}}=-\left[\frac{\hat{h}^3}{3\bar{\mu}(\phi)}\left(\hat{h}_{\hat{x}\hat{x}}+\hat{\Pi}\right)_{\hat{x}}\right]_{\hat{x}}, \tag{14}$$

$$\phi_{\hat{t}}=-\frac{\hat{h}^2}{3\bar{\mu}(\phi)}\phi_{\hat{x}}\left(\hat{h}_{\hat{x}\hat{x}}+\hat{\Pi}\right)_{\hat{x}}+\frac{1}{\hat{\mathrm{Pe}}}\frac{(\hat{h}\phi_{\hat{x}})_{\hat{x}}}{\hat{h}}, \tag{15}$$

where $\hat{\Pi}$ is given by

$$\hat{\Pi}=\hat{\mathcal{C}}\left[\bar{\Pi}_0\cos(\bar{\omega}\hat{h}+\varphi_2)e^{-\bar{\kappa}\hat{h}}+\bar{\Pi}_1e^{-\bar{\delta}(\hat{h}-1)}\right],\quad \text{for}\quad \hat{h}>1$$

$$=-\hat{C}\frac{6\phi}{\pi}\bar{P}+\frac{\hat{\mathcal{A}}}{\hat{h}^3}+\hat{\mathcal{B}}e^{-\hat{\lambda}\hat{h}},\quad \text{for}\quad 0<\hat{h}<1. \tag{16}$$

Estimates of the magnitudes of the dimensionless groups that appear in Eqs. (14)–(17) are provided in Table I. Inspection of this table reveals that the magnitude of electrostatic forces is small and they will be neglected in the remainder of this paper. In Fig. 1(a), we show the effect of varying the particle concentration on the structural component of the disjoining pressure. Clearly, increasing ϕ leads to the formation of a more pronounced peak at $\hat{h}=1$, oscillations of larger amplitude and longer decay length, and an increase in the magnitude of depletion forces, as expected. A comparison of the van der Waals and structural disjoining pressure components is shown in Fig. 1(b). Increasing the value of the reduced Hamaker constant leads to a concomitant increase in the magnitude of the van der Waals component and its decay length. Also noteworthy is the subdominance of the depletion forces in relation to the van der Waals interactions over the range $0<\hat{h}<1$, which is accentuated with decreasing $\hat{h}$. The depletion component of the disjoining pressure for $0<\hat{h}<1$ is therefore neglected and is not used to generate the results discussed in the following section. Note that the values of $\hat{\mathcal{A}}$ and $\hat{\mathcal{C}}$ used to plot the curves shown in Fig. 1 are chosen to be in the middle of the range of the values listed in Table I. We turn our attention to the discussion of the results. Note that the hat decoration is suppressed for the remainder of this paper with the understanding that reference will be made to the rescaled variables.

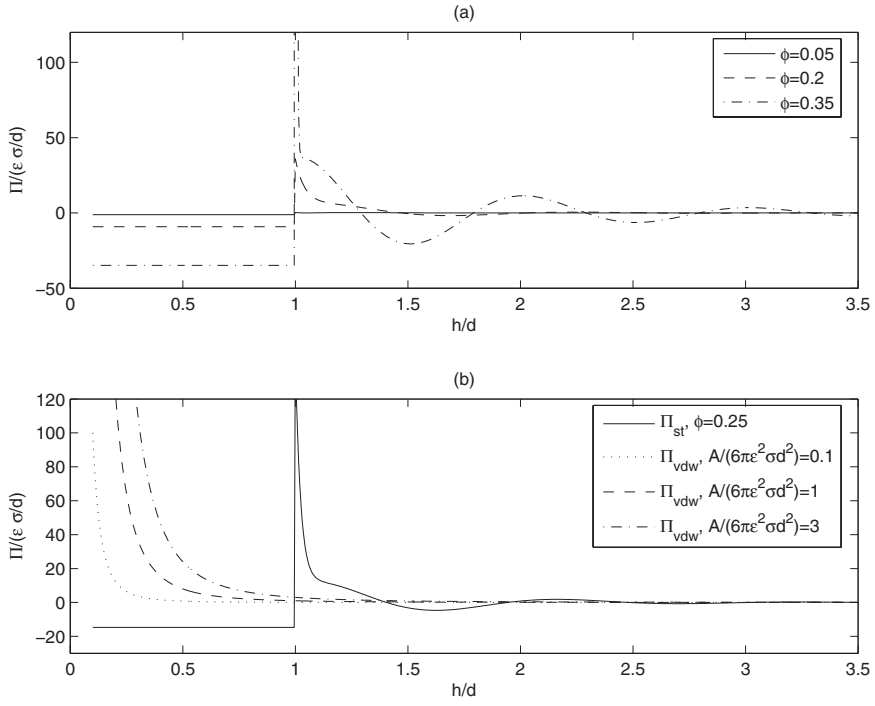

FIG. 1. Parametric dependence of the spatial variation of the structural disjoining pressure component on ϕ with $\hat{\mathcal{C}}=10$ (a), and a comparison of the spatial distributions of the van der Waals and structural (generated with $\hat{\mathcal{C}}=10$) components (b).

III. RESULTS

A. Numerical procedure

The evolution equations are solved using a numerical procedure that employs the finite-difference approximation to discretize the spatial derivatives: Centered differences are used over the whole of the computational domain except for the end points where one-sided differences are utilized. Typically, 5000 grid points are used to carry out the computations. Numerical solutions were obtained starting from the following initial condition:

$$\begin{aligned} &h(x,0) = 1 - 2x + h_\infty, \qquad \phi(x,0) = \phi_o \quad \text{for } -L_l \le x \le 0.5, \\ &h(x,0) = h_\infty, \qquad\qquad\quad \phi(x,0) = 0 \quad \text{for } 0.5 < x \le L_r, \end{aligned} \tag{17}$$

where $L_l=5$ and $L_r=200$. This is the linear initial profile in h with an offset in x so that a single particle depth ($h=1$) is at $x\sim 0$; also present is a small constant h_∞. Equation (17) models the situation in which the contact line region is represented by a particles-laden fluid wedge. The contact line singularity at the edge of this region is relieved by using a precursor layer of thickness h_∞, which is assumed to be devoid of particles. The value of $h_\infty=0.01$ is fixed for all the computations presented in this paper. Solutions are obtained subject to the following boundary conditions:

$$\begin{aligned} &h_x(-L_l,t) = -2, \qquad h(L_r,t) = h_\infty, \\ &h_{xxx}(-L_l,t) = 0, \qquad h_{xxx}(L_r,t) = 0, \\ &\phi_x(-L_l,t) = 0, \qquad \phi_x(L_r,t) = 0, \end{aligned} \tag{18}$$

for $0\le\phi_o\le 0.4$, $0\le\hat{\mathcal{C}}\le 15$, $1\le \mathrm{Pe}\le 10$, and $\hat{\mathcal{A}}=0.5$.

In this study, since the particulate phase influences the viscosity we shall take $\bar{\mu}=(1+\phi/2)$ for $0<\phi\le 0.1$. For $\phi>0.1$, we shall either use the Krieger-Dougherty relationship, $\bar{\mu}_{\mathrm{KD}}=(1-\phi/\phi_m)^{-2}$ for $0.1\le\phi\le\phi_m$ with $\phi_m=0.64$, or $\bar{\mu}_{\mathrm{fit}}=1-304.18\phi^6+360.13\phi^5+102.65\phi^4-274.93\phi^3+111.85\phi^2-14.35\phi$, which represents a fit of the viscosity dependence on the concentration in the work of MacKay *et al.* [34] that shows that the addition of nanoparticles can in certain cases decrease the suspension viscosity.

B. Spreading of a nanoparticulate drop

In Fig. 2, we show the spatiotemporal evolution of the film thickness h and the local particle mass $h\phi$ with $\phi_o=0.25$, $\hat{\mathcal{C}}=10$, $\hat{\mathcal{A}}=0.5$, and $\mathrm{Pe}=10$. It is clearly seen that the spreading process is accompanied by the formation of a well-pronounced step, which appears to grow at the "foot" of the advancing wedge close to $h=1$. This feature is brought about by the structural component of the disjoining pressure, due to the presence of nanoparticles in the film, which is particularly significant at $h=1$, as shown in Fig. 1. Below $h=1$, where a single layer of particles is present, structural disjoining pressure effects are absent and van der Waals forces are dominant. These forces are responsible for the decay in the film thickness from $h=1$ to $h=h_\infty$. The local particle mass, shown in Fig. 2(b), has a very similar shape to h. Only h profiles will therefore be presented henceforth.

We have also examined the effect of varying ϕ on the structure of the film thickness near the edge of the spreading drop. In Fig. 3(a), we show h profiles for $\phi\in[0,0.35]$ with the rest of the parameters remaining unchanged from Fig. 2. Inspection of Fig. 3(a) reveals that increasing ϕ_o, which corresponds to an increase in the relative significance of the structural component of the disjoining pressure, leads to the formation of more pronounced steps; this is in contrast to the situation in the absence of particles, $\phi=0$: In this case, the spreading is dominated solely by van der Waals forces and proceeds in the absence of step formation.

In order to measure the rate of the spreading process, we introduce the following integral measure:

$$0.95M = \int_{L_l}^{x_f} h dx, \tag{19}$$

where x_f is defined as the spatial location at which 0.95 of the total mass of liquid, $M\equiv\int_{L_l}^{L_r} h dx$, is recovered. In Fig. 3(b), we show the temporal evolution of x_f for the same parameter set as that used to generate Fig. 2; in particular, $\bar{\mu}_{\mathrm{KD}}$ was used to characterize the dependence of the viscosity on particle concentration. It is clearly seen that increasing ϕ_o leads to a decrease in the spreading rate, which is clearly caused by an increase in the viscosity due to the presence of the nanoparticles as dictated by the Krieger-Dougherty relation $\bar{\mu}_{\mathrm{KD}}$. At early times, however, the spreading rate associated with $\phi=0.05$ was found to be approximately equal to that in the absence of particles before the particles-induced viscosity increase led to its reduction. In Fig. 3(c), we show an analogous plot to that depicted in Fig. 3(b), except $\bar{\mu}_{\mathrm{fit}}$ was used instead of $\bar{\mu}_{\mathrm{KD}}$. Close inspection of Fig. 3(c) reveals that the spreading rate is maximized for an intermedi-

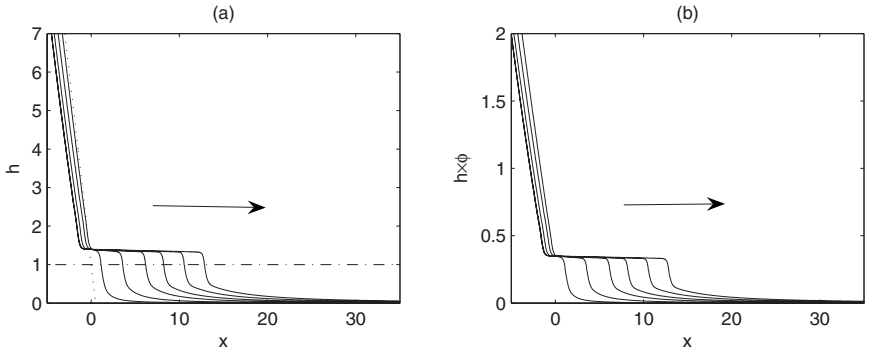

FIG. 2. Spatiotemporal volution of the film thickness (a) and local particle mass (b) for $\bar{\mu}=\bar{\mu}_{\mathrm{KD}}$, $\phi_o=0.25$, $\hat{\mathcal{C}}=10$, $\hat{\mathcal{A}}=0.5$, $\mathrm{Pe}=10$, and $t=0.28$, 2.8, 14, 36.4, 61.6, 98, 140; the arrows indicate the direction of increasing time and the dotted line in panel (a) demarcates the locus of points for which a single layer of particles is present.

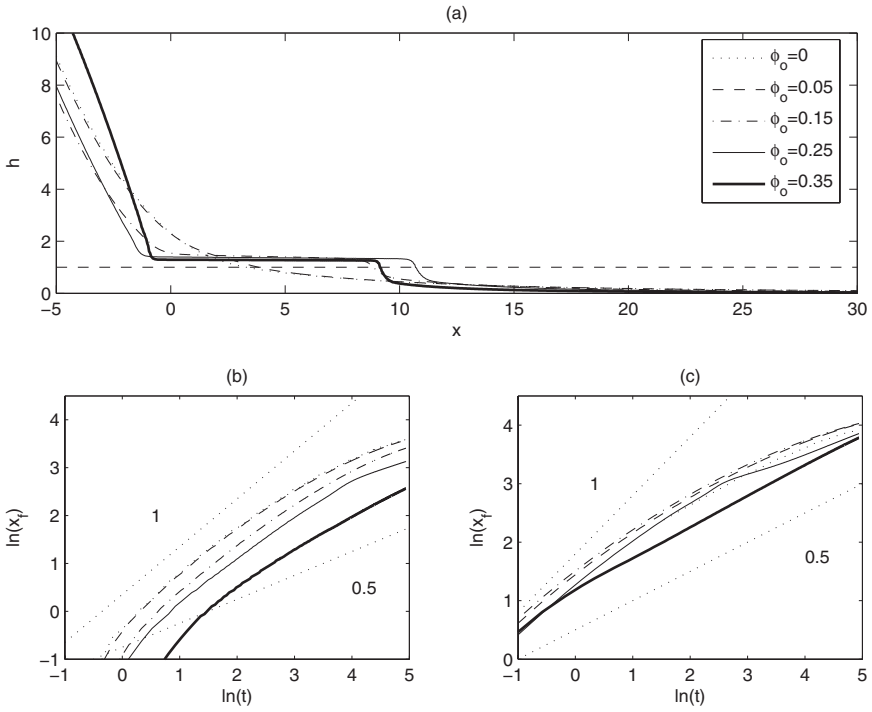

FIG. 3. (a): The effect of varying ϕ_o on the structure of the film thickness at $t=100$ with $\bar{\mu}=\bar{\mu}_{\mathrm{KD}}$. Log-log plots showing the temporal variation of x_f are depicted in (b) and (c) generated with $\bar{\mu}=\bar{\mu}_{\mathrm{KD}}$ and $\bar{\mu}=\bar{\mu}_{\mathrm{fit}}$, respectively. The dotted lines labeled "0.5" and "1" in (b) and (c) represent lines of constant slope equal to 0.5 and 1, respectively. The rest of the parameter values remain unchanged from Fig. 2.

ate value of ϕ_o, $\phi_o=0.15$ for the present set of parameters, and this is related to the lubricating effect of the nanoparticles, which act to reduce the viscosity [34]. A similar effect was recently observed in the forced spreading of thin films containing nanoparticles [39]. The spreading loosely follows a power-law-like behavior which is characterized by an exponent whose value approaches unity at intermediate times and decreases towards 0.5 with increasing ϕ_o.

We have also explored the effect of varying $\hat{C}$ on the dynamics. Increasing $\hat{C}$ was found to increase the spreading rate marginally without introducing qualitatively new features to the structure of the film thickness (not shown).

C. Terraced spreading of nanodroplets

An interesting and important feature of spreading is the emergence of a precursor layer from the edge of a droplet spreading on a wetting substrate and the "terracing" that is often also observed. Experiments on nanodroplets by Heslot *et al.* [1], and by later authors [2], demonstrate that the droplet spreads and flattens with a foot of approximately a molecular thickness emerging from the droplet; transient terracing events are observed with each terrace being of apparently equal thickness. We attempt below to replicate these dynamic phenomena, at least qualitatively, by neglecting the presence of particles and considering a decaying oscillatory, structural disjoining pressure of the form

$$\hat{\Pi} = \hat{C}\tilde{\Pi}_0 \cos(\tilde{\omega}h + \phi_2)\exp(-\tilde{\kappa}\hat{h}), \tag{20}$$

where $\tilde{\Pi}_0$, $\tilde{\omega}$, ϕ_2, $\tilde{\kappa}$ are constants; to the best of our knowledge, such an attempt does not appear to have been undertaken previously within the framework of thin-layer theory.

Relations of the form given by Eq. (20) are commonplace in studying the stepwise thinning of free films for foams [40]. Such oscillatory disjoining pressures are a feature of all fluids, composed of, say, a hard-sphere fluid model of larger molecules within a suspension of another fluid, or of ionic fluids [41] or of molecular solvents [17]. Even a seemingly pure high molecular weight fluid in experiments could be in this state if small amounts of, for instance, water were adsorbed to form the solvent. Thus one would expect adsorption of water onto either the substrate or its absorption by the fluid to have a potentially large effect, as observed experimentally by Villette *et al.* [42].

Since the presence of nanoparticles has been neglected in this part of the present work, d corresponds simply to a representative vertical scale of a typical nanodroplet and the results shown in Fig. 4 are for typical values; here, numerical solutions are obtained starting from an initial droplet profile given by $h(x,0)=\max(4-x^2,0)+h_\infty$ wherein $h_\infty=10^{-2}$ is, once again, used to relieve the contact line singularity; we have found the results to be insensitive to reducing this value further. As one immediately notes from the evolving h profiles and the disjoining pressure plots shown alongside these in Fig. 4, the terraces form for values of h such that $\Pi(h)=0$ and $\Pi_h<0$. One would expect to attain an equilibrium situation in cases wherein $\Pi(h)=0$ [or, in the study of "black hole" formation in foam films, for instance, when $\Pi(h)$ equals the applied capillary suction pressure [7], which is absent in the present case]. However, not all equilibrium states are stable: if $h=h_0+h_1\exp(ikx+\lambda t)$, with $h_1/h_0 \ll 1$, then linearization suggests that the perturbation growth rate λ is $\lambda=-[k^4-k^2\Pi_h]/3<0$, provided $\Pi_h<0$; this indicates that h_0 is stable to all perturbations of wave number k provided Π_h as expected [43]. The droplet spreads via the formation of a series of descending terraces until only the leading foot remains; this is reminiscent of the behavior observed in experiments [1].

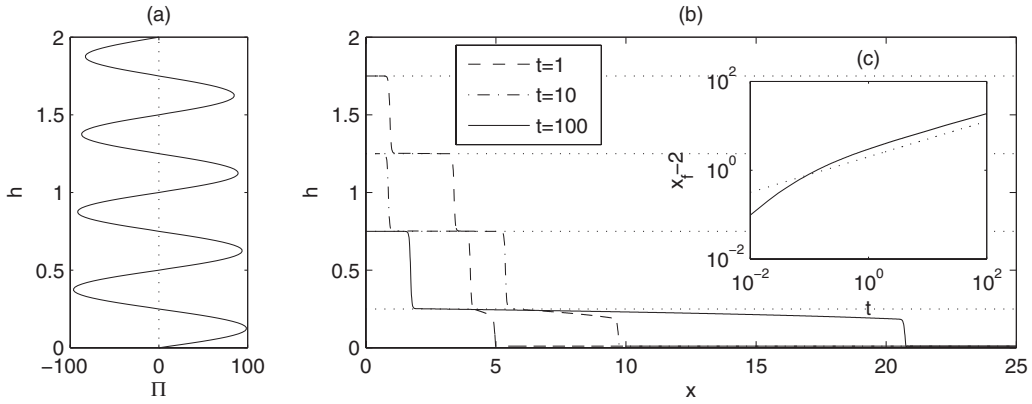

FIG. 4. Numerical simulation of "terraced spreading." (a) The variation of the disjoining pressure $\Pi(h)$, given by Eq. (20), and Π_h with h; (b) terrace formation in h for $t=1$, 10, 100 with $\hat{C}\tilde{\Pi}_0=100$, $\varphi_2=-\pi/2$, $\omega=4\pi, \kappa=0.1$ the dotted lines are those values of h for which $\Pi(h)=0$, $\Pi_h(h)<0$; (c) the temporal variation of the leading front x_f relative to the initial location of the droplet edge. Here, the dotted line, which has a slope of 0.4, has been included for comparison with $x_f-2\sim t^{0.4}$ power-law behavior.

Also shown in Fig. 4 is the edge of the leading terrace, relative to the initial droplet edge, versus time. This appears to scale as $t^{0.4}$ whereas experiments appear to show a $t^{0.5}$ scaling, albeit for early times and not for all fluids [42]. This feature has led some authors to view the motion of the terraces to be diffusive, although recent experiments [44] suggest otherwise. Nevertheless, it is clear that qualitative features of stepwise spreading and terracing can be captured within the framework of lubrication theory by incorporating an oscillatory disjoining pressure into equations governing the dynamics.

IV. CONCLUDING REMARKS

In this paper, we have considered the dynamic spreading of droplets containing nanoparticles. We have used lubrication theory to derive evolution equations for the film thickness and particle concentration, which account for the presence of the structural component of the disjoining pressure. Our numerical results indicate that the spreading is accompanied by the formation of a step at the advancing contact line, which is in line with recent experimental observations [15]. Our results also show that, by accounting for the potentially lubricating effect of the particles [34], the spreading rate is maximized for an intermediate value of the particle concentration; this is in agreement with recent experimental observations by one the authors [39]. We have also examined the possibility of replicating qualitatively the terracing phenomenon that has been observed to accompany the spreading of droplets [1]. Our numerical solutions of the film thickness equation with a decaying, oscillatory disjoining pressure $\Pi(h)$ bear structural resemblance to experimental observations. We show that thickness of the terraces corresponds to the zeros of the oscillatory dependence of $\Pi(h)$, provided $\Pi_h<0$, which guarantees stability.

The aim of our modeling has been to highlight features that dynamically appear provided structural disjoining pressures are introduced, and to begin to explore whether these models offer the possibility that terracing and step propagation can be captured within a continuum description. It is worthwhile to comment further upon the model, and its limitations. In the nanoparticulate droplet case, we have rescaled to the edge of the droplet and assumed that vertical diffusion is so rapid that the concentration is only a function of the horizontal coordinate which, in the neighborhood of the droplet edge, is a reasonable first approximation; clearly this could be modified at the expense of solving a two-dimensional convective-diffusion equation for the concentration to account for variations in the vertical direction. The modeling can be generalized in order to study the spreading of particle-laden polymeric fluids; the viscosity model of [34] is indeed for such fluids and is used here to demonstrate that one can have a nonmonotonic spreading rate behavior on particle concentration. Another limitation is that we have implicitly assumed that the substrate is hydrophilic by using a precursor layer as a numerical device to relieve the contact line singularity; this too could be overcome by adjusting the disjoining pressure further to mimic a contact angle at the edge of advancing step. Finally, the numerical simulations have all been in Cartesian geometry, local to the edge of a large droplet; this clearly captures the leading order behavior. For nanodroplets, it is less clear that this is so, and the modeling could be generalized to this too; indeed we did so, but for the sake of brevity do not show the results as they add nothing new to the thrust of this paper.

APPENDIX: CONSTANTS APPEARING IN EQ. (12)

Here, we provide details of the functional dependence of the various coefficients in Eq. (4) on ϕ [14]:

$$\beta\Delta\mu = \phi\frac{(8-9\phi+3\phi^2)}{(1-\phi)^3} \equiv \bar{F}(\phi), \tag{A1}$$

$$P = \rho kT\frac{(1+\phi+\phi^2-\phi^3)}{(1-\phi)^3} \equiv \frac{kT}{d^3}\frac{6\phi}{\pi}\bar{P}(\phi), \tag{A2}$$

$$\Pi_0 = \frac{kT}{d^3}(4.06281 - 3.10572\phi + 76.67\phi^2) \equiv \frac{kT}{d^3}\bar{\Pi}_0(\phi), \tag{A3}$$

$$\kappa = \frac{4.78366 - 19.64378\phi + 37.379\phi^2 - 30.59647\phi^3}{d} \equiv \frac{\bar{\kappa}(\phi)}{d}, \tag{A4}$$

$$\omega = \frac{4.45160 + 7.10586\phi - 8.30671\phi^2 + 8.29751\phi^3}{d} \equiv \frac{\bar{\omega}(\phi)}{d}, \tag{A5}$$

$$\varphi_2 = -0.39687 - 0.3948\phi + 2.3027\phi^2, \tag{A6}$$

$$\sigma_s = -\frac{9kT}{2\pi d^2}\phi^2\frac{(1+\phi)}{(1-\phi)^3} \equiv = -\frac{kT}{d^2}\bar{\sigma}_s, \tag{A7}$$

$$\varphi_1 = 0.40095 + 2.10336\phi, \tag{A8}$$

$$W_0 = \frac{kT}{d^2}(0.57909 + 0.83439\phi + 8.65315\phi^2) \equiv \frac{kT}{d^2}\bar{W}_0, \tag{A9}$$

$$\Pi_1 = \frac{kT}{d^3}\left[\frac{6\phi}{\pi}(e^{\bar{F}} - \bar{P}) - \bar{\Pi}_0 e^{-\bar{\kappa}}\cos(\bar{\omega} + \varphi_2)\right] \equiv \frac{kT}{d^3}\bar{\Pi}_1, \tag{A10}$$

$$\delta = \frac{\bar{\Pi}_1}{d[2\bar{\sigma}_s - \bar{W}_0 e^{-\bar{\kappa}}\cos(\bar{\omega} + \varphi_1)]} \equiv \frac{\bar{\delta}}{d}. \tag{A11}$$

[1] F. Heslot, N. Fraysse, and A. M. Cazabat, Nature (London) **338**, 640 (1989).
[2] S. Betelu, B. M. Law, and C. C. Huang, Phys. Rev. E **59**, 6699 (1999).
[3] A. D. Nikolov and D. T. Wasan, J. Colloid Interface Sci. **133**, 1 (1989).
[4] A. D. Nikolov, P. A. Kralchevsky, I. B. Ivanov, and D. T. Wasan, J. Colloid Interface Sci. **133**, 13 (1989).
[5] A. D. Nikolov, D. T. Wasan, N. D. Denkov, P. A. Kralchevsky, and I. B. Ivanov, Prog. Colloid Polym. Sci. **82**, 87 (1990).
[6] D. T. Wasan, A. D. Nikolov, P. A. Kralchevsky, and I. B. Ivanov, Colloids Surf. **67**, 139 (1992).
[7] V. Bergeron and C. J. Radke, Langmuir **8**, 3020 (1992).
[8] V. Bergeron, A. J. Jimenez-Laguna, and C. J. Radke, Langmuir **8**, 3027 (1992).
[9] X. L. Chu, A. D. Nikolov, and D. T. Wasan, J. Chem. Phys. **103**, 6653 (1995).
[10] X. L. Chu, A. D. Nikolov, and D. T. Wasan, J. Chem. Phys. **105**, 4892 (1996).
[11] D. Henderson, S. Sokolowski, and D. T. Wasan, J. Stat. Phys. **89**, 233 (1997).
[12] S. Manne and G. Warr, eds., *Supramolecular structures in confined geometries* (American Chemical Society, Washington, DC, 1999).
[13] R. L. Kao, D. T. Wasan, A. D. Nikolov, and D. A. Edwards, Colloids Surf. **34**, 389 (1989).
[14] A. Trokhymchuk, D. Henderson, A. Nikolov, and D. T. Wasan, Langmuir **17**, 4940 (2001).
[15] D. T. Wasan and A. D. Nikolov, Nature (London) **423**, 156 (2003).
[16] A. Chengara, A. D. Nikolov, D. T. Wasan, A. Trokhymchuk, and D. Henderson, J. Colloid Interface Sci. **280**, 192 (2004).
[17] J. N. Israelachvili, *Intermolecular and Surface Forces* (Academic Press, San Diego, CA, 1992).
[18] N. V. Churaev, Adv. Colloid Interface Sci. **103**, 197 (2003).
[19] A. Oron, S. H. Davis, and S. G. Bankoff, Rev. Mod. Phys. **69**, 931 (1997).
[20] R. V. Craster and O. K. Matar (unpublished).
[21] M. R. E. Warner, R. V. Craster, and O. K. Matar, Phys. Fluids **14**, 4040 (2002).
[22] A. Sharma, Eur. Phys. J. E **12**, 397 (2003).
[23] A. Sharma and E. Ruckenstein, J. Colloid Interface Sci. **113**, 456 (1986).
[24] W. W. Zhang and J. R. Lister, Phys. Fluids **11**, 2454 (1999).
[25] M. R. E. Warner, R. V. Craster, and O. K. Matar, Phys. Fluids **14**, 1642 (2002).
[26] U. Thiele, K. John, and M. Bar, Phys. Rev. Lett. **93**, 027802 (2004).
[27] A. Sharma and R. Khanna, Phys. Rev. Lett. **81**, 3463 (1998).
[28] A. Sharma and R. Khanna, J. Chem. Phys. **110**, 4929 (1999).
[29] S. Asakura and F. Oosawa, J. Chem. Phys. **22**, 1255 (1954).
[30] R. Kjellander and S. Sarman, Chem. Phys. Lett. **149**, 102 (1988).
[31] P. Attard and J. L. Parker, J. Phys. Chem. **96**, 5086 (1992).
[32] P. A. Kralchevsky and N. D. Denkov, Chem. Phys. Lett. **240**, 385 (1995).
[33] B. Götzelmann, R. Evans, and S. Dietrich, Phys. Rev. E **57**, 6785 (1998).
[34] M. E. MacKay, T. T. Dao, A. Tuteja, D. L. Ho, B. van Horn, H.-C. Kim, and C. Hawker, Nat. Mater. **2**, 762 (2003).
[35] P. Attard, D. R. Bérard, C. P. Ursenbach, and G. N. Patey, Phys. Rev. A **44**, 8224 (1991).
[36] O. E. Jensen and J. B. Grotberg, Phys. Fluids A **5**, 58 (1993).
[37] L. W. Schwartz and R. R. Eley, J. Colloid Interface Sci. **202**, 173 (1998).
[38] L. Y. Yeo, R. V. Craster, and O. K. Matar, J. Colloid Interface Sci. **306**, 368 (2007).
[39] K. Sefiane, J. M. Skilling, J. MacGillivray, *Proceedings of the 10th UK heat Transfer Conference*, edited by K. Sefiane and P. Kew (Edinburgh, 2007).

[40] C. Stubenrauch and R. von Klitzing, J. Phys.: Condens. Matter **15**, R1197 (2003).
[41] D. Henderson, D. T. Wasan, and A. Trokhymchuk, J. Chem. Phys. **119**, 11989 (2003).
[42] S. Villette, M. P. Valignat, A. M. Cazabat, L. Jullien, and F. Tiberg, Langmuir **12**, 825 (1996).
[43] A. Sharma, Langmuir **9**, 861 (1993).
[44] H. Xu, D. Shirvanyants, K. Beers, K. Matyjaszewski, M. Rubinstein, and S. S. Sheiko, Phys. Rev. Lett. **93**, 206103 (2004).